NAD^+ flux is maintained in aged mice

Melanie McReynolds
Princeton University https://orcid.org/0000-0001-5427-2739
Karthikeyani Chellappa
Perelman School of Medicine, University of Pennsylvania,
Eric Chiles
Rutgers University
Connor Jankowski
Lewis-Sigler Institute for Integrative Genomics, Department of Chemistry, Princeton University, Princeton NJ https://orcid.org/0000-0003-1247-4548
Yishui Shen
Princeton Univeristy
Li Chen
Princeton University https://orcid.org/0000-0001-8685-3466
Helene Descamps
University of Pennsylvania
Sarmistha Mukherjee
University of Pennsylvania
Yashaswini Bhat
University of Pennsylvania
Qingwei Chu
University of Pennsylvania
Paul Botolin
University of Pennsylvania
Cristoph Thaiss
Microbiology Department, Institute for Immunology, and Institute for Diabetes, Obesity & Metabolism, Perelman School of Medicine, University of Pennsylvania, Philadelphia, Pennsylvania
https://orcid.org/0000-0001-8226-7718
Wenyun Lu
Princeton University
Xiaoyang Su
Rutgers University https://orcid.org/0000-0001-8081-1396
Joshua Rabinowitz
Princeton University https://orcid.org/0000-0002-1247-4727
Joseph Baur (baur@pennmedicine.upenn.edu)

University of Pennsylvania https://orcid.org/0000-0001-8262-6549

Article

Keywords: NAD+ flux, isotope tracing, mass spectrometry, aged mice

Posted Date: October 9th, 2020

DOI: https://doi.org/10.21203/rs.3.rs-86538/v1

Abstract

NAD^+ is an essential coenzyme found in all living cells. NAD^+ concentrations decline during aging, but whether this reflects impaired production or accelerated consumption remains unclear. Here we employed isotope tracing and mass spectrometry to probe NAD^+ metabolism across tissues in aged mice. In 25-month-old mice, we observe modest tissue NAD^+ depletion (median decrease ~ 30%) without significant changes in circulating NAD^+ precursors. Isotope tracing showed unimpaired synthesis of circulating nicotinamide from tryptophan, and maintained flux of circulating nicotinamide into tissue NAD^+ pools. Although absolute NAD^+ biosynthetic flux was maintained in most tissues of aged mice, fractional tissue NAD^+ labeling from infused labeled nicotinamide was modestly accelerated, consistent with increased activity of NAD^+ consuming enzymes. Long-term calorie restriction partially mitigated age-associated NAD^+ decline despite decreasing NAD^+ synthesis, suggesting that calorie restriction reduces NAD^+ consumption. Thus, age-related decline in NAD^+ is relatively subtle and driven by increased NAD^+ consumer activity rather than impaired production.

Introduction

Aging is the strongest risk factor for the most prevalent diseases in developed nations, including diabetes, cancer, cardiovascular, and neurodegenerative disorders. Demographics are projected to continue to shift toward a higher proportion of aged individuals, making it imperative to identify strategies to promote healthier aging. Nicotinamide adenine dinucleotide (NAD^+) is an essential coenzyme in redox reactions and co-substrate for signaling enzymes (Pollak, 2007; Srivastava, 2016; Yang, 2016). NAD^+ decreases in concentration with age in worms, flies, mice and humans (Chini, 2017; Gomes, 2013; McReynolds MR, 2020; Mouchiroud, 2013; Yoshino J, 2018; Zhang, 2016). NAD^+ depletion causes multiple defects including mitochondrial dysfunction, deregulated nutrient sensing, and epigenetic alterations, which are classic hallmarks of aging (Gomes, 2013; Salvatori, 2017; Verdin, 2015). Moreover, supplementation of the NAD^+ pool is simple, appears to be safe, and has beneficial effects in aged mice (Mills, 2016; Zhang, 2016). Thus, decreased NAD^+ availability may be a contributing and modifiable factor in age-related diseases. Although several mechanisms have been proposed to contribute to either decreased synthesis of NAD^+ or increased consumption during aging, the reason for the decline remains incompletely understood and the net effect on flux through NAD^+-dependent reactions has not been determined.

NAD^+ is best known for its role as an oxidoreductase cofactor; by accepting and donating hydride ions (H^-). NAD^+ plays a central role in metabolism, carrying high-energy electrons to support myriad biochemical reactions including those that drive glycolysis, oxidative phosphorylation and β-oxidation (Pollak, 2007). However, NAD^+ also serves as a co-substrate for signaling enzymes that can modulate metabolic and transcriptional responses, including the sirtuins (SIRTs), poly ADP-ribose polymerases (PARPs), cyclic ADP-ribose synthases (CD38/CD157), mono ADP-ribosyltransferases, and Sterile Alpha and Toll/interleukin-1 Receptor Motif-Containing 1 (SARM1). These enzymes continuously degrade NAD^+

and release nicotinamide (NAM), necessitating a means to replenish the NAD^+ pool (McReynolds MR, 2020). In mammals, NAD^+ is made *de novo* from tryptophan and via the Preiss-Handler pathway from nicotinic acid, but the bulk of synthesis in most tissues occurs via the salvage pathway from NAM (Liu L, 2018) (Figure S1A). Thus, the balance between NAD^+ consumption and synthesis from NAM determines the steady state concentration in most tissues.

A decrease in NAD^+ concentration with age could be driven by either an increase in consumer activity or a decrease in synthesis. It has been proposed that increased PARP activity, potentially as a direct result of increased DNA damage, could drive age-related NAD^+ decline, and inhibition of PARPs is sufficient to block NAD^+ depletion and premature aging in a mouse model with defective DNA repair (Bai P, 2011; E.F. Fang, 2014; Scheibye-Knudsen M, 2014; Wang, 2014). In contrast, data have been presented to support the model that CD38 is the primary cause of age-related NAD^+ decline. CD38 is expressed primarily by immune cells, and increased immune cell infiltration, CD38 expression and activity are observed in aged tissues (Tarragó MG, 2018). Moreover, CD38 knockout mice have elevated NAD^+ that does not appear to decline with age in multiple tissues (Tarragó MG, 2018). These observations support increased consumer activity as the driver of age-related NAD^+ decline via inflammation (CD38) (Amici SA, 2018; Camacho-Pereira, 2016; Chini C, 2019; Kang BN, 2006; Matalonga J, 2017; Musso T, 2001) or DNA damage (PARP1) (Massudi, 2012; Scheibye-Knudsen M, 2014; Ubaida-Mohien C, 2019). On the other hand, mRNA and protein expression of nicotinamide phosphoribosyltransferase (Nampt), the rate-limiting enzyme in the NAD^+ salvage pathway, is reduced with age in multiple tissues (Mills, 2016; Stein LR, 2014). Similarly, levels of extracellular NAMPT in circulation decline with age in mice and humans (Yoshida M, 2019). The second step of the NAD^+ salvage pathway is catalyzed by three isoforms of nicotinamide mononucleotide adenylyl transferase (NMNAT). Aged liver exhibits a significant decline in mRNA expression of *Nmnat1* and trends towards lower expression of *Nmnat2* and *Nmnat3* (Camacho-Pereira, 2016). Similarly, expression levels of NMNAT isoforms are reduced in the kidneys, oocytes and colons of aged mice (Guan Y, 2017; Wu X, 2019; Zhu X, 2017). These observations suggest the alternative hypothesis that NAD^+ decline could be driven at least in part by decreased synthesis. At present, it remains unclear whether consumption or synthesis is the primary driver of age-related decline in NAD^+ availability. Differentiating these possibilities may allow more targeted therapeutic strategies to restore or boost NAD^+ level and slow down age-related cellular process. However, steady state concentration measurements are ill-suited to this task. Thus, there is a need to examine NAD^+ metabolic flux, i.e., the rates of production and degradation of the NAD^+ chemical backbone in aged tissues.

To this end, we employed isotope-labeled NAD^+ precursors, mass spectrometry, and quantitative modeling to determine NAD^+ fluxes in young and aged mice. We first established an in-depth repertoire of the NAD^+ metabolome across tissues. We confirmed that NAD^+ pools are reduced modestly with age in some, but not all of twenty one tissues examined. Our data establish that NAD^+ synthesis rates are maintained with age, despite lower steady-state concentrations, pointing to increased consumer activity as the primary driver of age-related NAD^+ decline. In contrast, life-long caloric restriction curtailed NAD^+

synthesis in most tissues, while steady-state concentrations were maintained or increased, indicating a decrease in consumer activity. Thus, our study demonstrates that aging and caloric restriction have opposing effects on NAD^+ consumption, and establishes a foundation for understanding how NAD^+ homeostasis is altered throughout the body during aging.

Results

NAD^+ metabolism is altered with age

We first established the steady-state NAD^+ metabolome in tissues of young (3mo) and aged (25mo) C57BL/6 mice from the National Institute of Aging (NIA)'s aged rodent colony (Figure 1A). NAD^+ and $NADP^+$ modestly declined with age in most tissues, with the degree of change being highly tissue-dependent (Figure 1B-E). NAD^+ pools were significantly decreased in the livers, kidneys, skeletal muscles, and adipose tissues of aged mice, consistent with prior literature. We also detected decreases in NAD^+ with age in the small intestine and colon, which to our knowledge have not previously been reported (Figure 1B and S1B). In contrast, the reduced forms of each nucleotide, NADH and NADPH, were much less affected by age, declining significantly only in the liver (Figure S1C). NADH and NADPH concentrations even trended upwards in some tissues with age, but this reached significance only for brain (Figure 1C-E, S1C). The oxidized form of $NADP^+$ was also increased with age in brain, indicating a net increase in the size of the total $NADP^+$ + NADPH pool.

We next examined the ratio of oxidized to reduced NAD(H) and NADP(H) in each tissue with age. These measures of whole tissue metabolite concentrations do not capture specific information on compartmentalization or "free" ratios available to enzymes within the cells, but may provide insight into whether gross changes in redox balance occur in aged tissues. A more reduced NAD(H) redox state with age has previously been reported for multiple tissues in rats (Braidy N, 2011), in human brains (Zhu XH, 2015), and in human plasma (Clement J, 2019). Consistently, tissue NAD/NADH ratios confirmed a general trend toward a more reduced redox state with age, with only the brain, soleus and jejunum reaching statistical significance (Figure S1D). A notable exception was the liver, which exhibited a significantly more oxidized redox state with age (Figure S1D, E). The decrease in NAD^+ with age was not solely attributable to a redox shift, as total abundance of NAD^+ + NADH was reduced in the aged liver, kidney, muscle and brown adipose tissue (Figure S1F). Thus, our findings support tissue-specific changes in both the abundance and redox states of the NAD(H) and NADP(H) pools with age in mice.

These changes in NAD(H) and NADP(H) levels in aged mice occurred without any consistent change in circulating NAM, the major NAD^+ precursor for most tissues (Figure S1G). In addition, there was no alteration in circulating levels of methylated NAM, the primary catabolic product of nicotinamide, which is eventually oxidized and excreted in the urine (Figure S1H). Circulating NR levels were also unchanged with age (Figure S1I), and NMN was not consistently detected in serum samples using our methodology. We further quantified tissue levels of NAD^+-related metabolites and precursors, noting trends of increased

NA and kynurenine, and decreased NMN across multiple tissues (Figure 1F). Thus, we find that aging leads to a decrease in the concentration of NAD^+ and alters related metabolites in some tissues without major changes in the abundance of circulating precursors.

Flux from tryptophan to circulating NAM is not altered with age

The liver consumes dietary tryptophan to synthesize NAD^+ via the *de novo* pathway and releases NAM, which serves as precursor for NAD^+ synthesis in other tissues via the salvage pathway (Liu L, 2018). Kynurenine is an intermediate in the *de novo* pathway that can also be released into the circulation and can influence immunological and neurological phenotypes independently from NAD^+ synthesis. We found that circulating Trp and kynurenine levels across the diurnal cycle were not altered with age (Figure 2A, B). However, only a small proportion of Trp is used for NAD^+ synthesis (Shibata, 2018), meaning that substantial changes in flux might be hard to detect at the level of Trp concentration. To test whether *de novo* NAD^+ synthesis from tryptophan was deranged with age, we employed isotope tracing to quantify NAD^+ production. [U-^{13}C]-Trp (M+11) was infused at a constant rate of 2.5 nmol/g/min for 15 hours, achieving serum enrichment of ~60% (M+11) tryptophan in both young and aged mice (Figure 2C, D). This was mirrored by similar enrichment (M+10) in the kynurenine pool (Figure 2E), and resulted in slower appearance of the downstream metabolites 3-hydroxyanthranilic acid (3HAA, M+6) and NAM (M+6) (Figure 2F, G). In all cases, the labeling patterns were indistinguishable between old and young animals. To determine whether age-associated changes in intestinal metabolism influences NAD synthesis from tryptophan, we infused [U-^{13}C]-Trp (M+11) using oral catheters. Again, we found no evidence for a difference between young and old animals (Figure S2A-M). Labeled NAM (M+6) and NAD^+ (M+6) from tryptophan were highly enriched in liver and appeared in most other tissues with similar kinetics in young and aged mice (Figure 2H, I). Altogether, our results indicate that synthesis of NAD^+ and secretion of NAM from tryptophan is unaltered with age (Figure S2N).

NAD^+ turnover is maintained with age

To investigate the effect of aging on NAD^+ synthesis from circulating NAM, we next infused [2,4,5,6-^{2}H]-NAM at a constant rate of 0.2 nmol/g/min (Figure 3A). We reasoned that the lower steady-state NAD^+ concentrations in aged animals could be driven by a decline in the activity of biosynthetic enzymes, or increase in the activity of consuming enzymes, or a combination of both. Moreover, metabolic flux will shift to some degree to resist changes in the concentration of a given metabolite, i.e., a fall in NAD^+ concentration will tend to increase the rate of synthesis (due to a lack of feedback inhibition) and tend to decrease consumption (due to its lower availability as a substrate) (Brand, 1997). In particular, we have demonstrated that NAD^+ consumption follows approximately first order kinetics in T47D cells (Liu L, 2018), implying a high dependence on NAD^+ concentration. Thus, we predict that a defect in synthesis of NAD^+ would cause the concentration to fall until the rate of consumption balances the new, lower synthesis rate (a net decrease in turnover), whereas an increase in consumer activity would cause NAD^+ concentration to fall with maintained or increased synthesis rates (reaching steady-state when the

concentration falls enough to bring NAD^+ consumption back in balance with synthesis, which will be maintained or increase as NAD^+ concentration falls). Infusion of labeled NAM allows us to distinguish these possibilities, which cannot be achieved using steady-state measurements.

An advantage of the specific deuterated NAM (M+4) used here is that one of the deuterium atoms is at the redox active (4-) position. This label remains associated with free NAM, but is rapidly lost upon incorporation into NAD^+, at which point the NAM moiety is capable of accepting and releasing hydride ions. Subsequent turnover of the labeled NAD^+ releases NAM (M+3). Thus, the appearance of NAM (M+3) in the blood serves as an index of whole-body NAD^+ turnover. While the fraction of (M+3) was too small and variable to interpret at early time points during the infusion, it was significantly higher in the aged animals by 21 hours (Figure 3B and S3A, B), suggesting that there is a small net increase in NAD^+ turnover with age, despite the lower NAD^+ concentrations available in many tissues. Furthermore, the circulatory flux of NAM is unaltered with age (Figure S3C) and the infusion caused only a modest increase in tissue NAM levels without affecting NAD^+ concentration in the liver and quadriceps muscle (Figure S3H).

To determine flux in specific tissues, we next examined the labeling patterns at different times after the start of infusion. By 24 hours, there was an increase in the fractional labeling of recycled NAM (M+3), but not M+4 NAM in the majority of aged tissues (Figure S3D, E). The fractional labeling of NAD^+ followed a similar trend, reaching significantly higher values by 24 hours in majority of the aged tissues (Figure 3C, D). Similarly, we detected an increase in the fractional labeling of nicotinamide mononucleotide (NMN), an intermediate in NAD^+ synthesis, from NAM (Figure S3F), and NADP (Figure S3G). Given the modestly smaller NAD^+ pool size in aged tissues, our data are consistent with unchanged or slightly increased absolute rates for NAD^+ synthesis and breakdown in most tissues, due to faster turnover of a smaller NAD^+ pool.

Inferring the precise differences in flux parameters between old and young mice can be difficult due to the partial and changing labeling patterns for tissue metabolite pools and the cyclical nature of the reactions involved. Thus, we next turned to quantitative modeling to extract fluxes and half-lives for NAM and NAD^+ across tissues. The flux model assumes both spatial homogeneity and metabolic steady state, where ($f1$ represents the Trp à NAD^+ flux, $f2$ represents NAM uptake and $f3$ represents NAM à NAD^+ flux (Figure 3E) (Liu L, 2018). For the majority of the young and aged tissues, the model was able to fit the experimental data with minimum error. NAD^+ turnover flux (sum of $f1$ + $f3$) was not significantly different between young and old tissues, with the exception that older spleens displayed higher turnover and older pancreas displayed lower turnover (Figure 3G, Table 1, Table SI). Thus, NAD^+ flux is largely maintained with age despite the lower NAD^+ pools sizes in some tissues (Figure 3E, F). A caveat that limits the precision of the modeling is that label incorporation is driven by a combination of NAM uptake and NAD^+ flux. When NAD^+ flux is fast relative to NAM uptake, the uptake rate ($f2$) becomes the dominant determinant of labeling intensity. Interestingly, while the NAD^+ synthesis flux ($f1$ + $f3$) is maintained in most aged tissues,

the NAM uptake flux (*f*2) is decreased in many aged tissues (Figure 3F, Table SI). We hypothesized that the NAM uptake flux is a major contributor to the differences in the labeling kinetics between young and aged tissues. To test this hypothesis, we simulated the labeling patterns of NAD^+ and NAM in the aged tissue by assuming that the NAD^+ synthesis flux values (*f*1 + *f*3) were identical to those of the young animals, and that only the NAM uptake flux (*f*2) changed to the rate calculated from aged tissue data (Figure S3H, S3I). The simulated labeling data using this method fit the aged tissue labeling patterns as well as when all three fluxes are allowed to vary, with the exceptions of spleen and pancreas (Figure S3H-J). This suggests that changes in NAM uptake and release fluxes may influence NAD^+ metabolism in aged tissues. Overall our data support the maintenance of absolute NAD^+ fluxes with age, with tissues that have smaller NAD^+ pools sizes generally turning over those pools modestly faster.

NAM base-exchange is not a major route of label incorporation into NAD^+

Several NAD^+ consuming enzymes also have the potential to catalyze a base-exchange reaction, whereby free NAM replaces the NAM moiety on NAD^+ (Behr A, 1981; Sauve AA, 1998; Sauve AA, 2003). Such reactions have no net consequence to the NAD^+ pool within the cell, but could result in label transfer, artificially creating the appearance of new NAD^+ synthesis. This mechanism was not a major contributor to NAD^+ labeling in T47D cells in culture (Liu L, 2018), since turnover rates calculated based on labeling rates agreed almost precisely with those obtained by inhibiting synthesis. However, the occurrence and physiological relevance of base-exchange reactions across tissues *in vivo* are not known.

To directly test the possibility that base-exchange of the deuterium-labeled NAM with unlabeled NAD^+ was confounding our measurements of labeled NAD^+, we performed an additional set of tracing studies in which young and aged mice were treated with the Nampt inhibitor FK866 prior to infusion (Figure 4A, S4A). Total circulating NAM pool accumulated in FK866 treated mice, as expected due to decreased utilization by NAMPT (Figure S4B, C). Importantly, the appearance of M+3 NAM was almost completely abolished in FK866 treated mice, indicating that the majority of NAD^+ labeling in infused animals is a direct result of synthesis, rather than base exchange (Figure 4B). Next, we examined the effects of FK866 treatment on NAD^+ labeling in tissues of young and aged mice. In all tissues, the appearance of labeled NAD^+ (M+3) was greatly reduced in the presence of FK866, confirming that NAMPT-dependent salvage synthesis, rather than base exchange, accounts for NAD^+ labeling from NAM (Figure 4C). As expected, this resulted in significant declines in tissue NAD^+ concentrations, with more pronounced effects in tissues with short NAD^+ half-lives (Figure 4D). Consistently, the fractional labeling of NMN, an intermediate in salvage synthesis that would not be labeled by base-exchange, correlated closely with labeling of NAD^+ across tissues and treatments (Figure 4E, F). NMN and NAD labeling was similar between young and aged mice treated with FK866. Together, these findings demonstrate that NAM base-exchange plays a minor role, if any, in generating the NAD^+ labeling patterns in our experiments.

Life-long caloric restriction curtails NAD^+ turnover

Caloric restriction (CR) is the most robust and reproducible intervention known to increase lifespan and healthspan across species (Anderson and Weindruch, 2012; Mattison et al., 2017). Short-term CR treatment increases steady-state NAD^+ levels in liver, adipose, and muscle tissues in young rodents (Chen D, 2008; Song J, 2014). This increase is correlated with upregulation of NAMPT in muscle (Song J, 2014), and key benefits of CR have been attributed to the actions of NAD^+-dependent sirtuin enzymes (Chalkiadaki and Guarente, 2012; Chen et al., 2005; Someya et al., 2010), suggesting the model that CR works in part by driving an increase in NAD^+ production and turnover. On the other hand, CR is well-known to decrease DNA damage and inflammation (SR, 2010), which would be expected to decrease NAD^+ consumption flux through PARPs and CD38, respectively. Thus, in CR, as in aging, NAD^+ flux could be predicted to increase or decrease, and the available steady-state measurements are incapable of resolving the question. Therefore, we investigated how NAD^+ metabolism was altered in mice subjected to life-long CR.

To directly examine the effect of life-long CR on NAD^+ flux, we infused three groups of animals: young (4 mo), aged (24 mo) and aged mice subjected to 40% CR from 4 months of age. Deuterium-labeled NAM was infused at a consistent rate of 0.2 nmol/g/min for 12 hours (Figure 5A). Similar enrichment of NAM (M+4) was achieved across all three groups. The appearance of NAM (M+3) in the circulation was not significantly different between the three groups, possibly owing to the low fractional enrichment and inter-individual variability at this time point (Figure 5B). However, we did observe differences in the NAD^+ pool sizes and labeling fractions within tissues. CR restored NAD^+ concentration in liver and increased it beyond the young level in white adipose tissue, but in contrast to prior reports in young rodents, did not have a major effect in aged skeletal muscle (Figure 5C). Newly synthesized (M+3) NAD^+ appeared more slowly in tissues from CR animals, indicating significantly decreased turnover across kidney, quad, eye cup, and white-adipose tissue, with similar non-significant trends in spleen and ileum (Figure 5D). $NADP^+$ turnover was also curtailed in CR animals, especially in the ileum (Figure 5E). We also sorted immune cell subsets from spleen, which revealed a more pronounced decline in steady-state NAD^+ concentration in B cells and a trend towards decline in T cells (Figure 5G-I), and an age-related increase in NAD^+ turnover in myeloid cells (Figure 5F). Changes in NAD^+ pool size and turnover in aged mice were prevented by CR. Together, these data reveal that CR curtails NAD^+ turnover rate in multiple aged tissues, and increases steady-state concentration in liver, and white adipose.

Turnover of mitochondrial NAD^+

The mitochondrial NAD^+ pool is distinct, as evidenced by several studies indicating that the organelles can retain their NAD^+ at least transiently when nuclear and cytosolic NAD^+ are depleted (C.A. Sims, 2018; Pittelli M, 2010; Yang H, 2007). We have previously demonstrated ongoing import of NAD^+ into mitochondria using heavy isotope labeling methods (Davila A, 2018), and shown that chronic lowering of NAD^+ concentration in skeletal muscle has a corresponding effect on NAD^+ concentration in the mitochondria (Frederick DW, 2016). To determine whether aging and CR have distinct effects on

mitochondrial NAD^+, we isolated mitochondria from the liver, kidney, and quadriceps muscles (Figure 6A). NAD^+ levels in the mitochondria were not significantly decreased with age, but trended lower in the skeletal muscle and kidney (Figure 6C-E). Total mitochondrial NAD^+ content was significantly increased by CR only in the liver. Labeling patterns for mitochondrial NAD^+ almost perfectly mirrored those in bulk tissues, except that the fractional labeling was 10-20% lower in each case (Figure 6B). This is consistent with either mitochondrial import of NAD^+ and dilution by the unlabeled pool, or with slightly slower turnover of NAD^+ synthesized inside the mitochondria. However, we view the latter case as unlikely, given the tight correlation with total tissue labeling and evidence that cytosolic NAD^+ can be imported into the organelles (Davila A, 2018). Together, these data provide some of the first insight into mitochondrial NAD^+ turnover *in vivo*.

Discussion

NAD^+ is critical to the maintenance of cellular homeostasis, with roles in energy balance, stress responses, epigenetics, DNA repair, immune response and a host of metabolic reactions. Hence, perturbations to the NAD^+ pool have the potential to trigger accelerated metabolic decline and may contribute to age-associated aliments (Mills, 2016; Zhang, 2016). Although age-related NAD^+ decline has been documented in numerous studies, there is no clear consensus as to the underlying causes, or even whether the primary driver is increased consumption or impaired synthesis. Here, we present a quantitative flux analysis of NAD^+ metabolism with age. A caveat to these studies, as with any tracer infusion, is that we are perturbing the circulating concentrations of the metabolites of interest. While blood levels of NAM increased 2-3-fold over the course of infusions, we note that tissue levels of NAM and NAD^+ were generally quite similar between infused and uninfused animals, supporting the view that our labeling strategy was minimally perturbative (Figure S3H). Thus, our data support the view that NAD^+ synthesis and turnover rates do not decline significantly – instead, aged tissues with lower NAD^+ concentrations generally have correspondingly faster fractional turnover such that total flux is preserved.

The most direct interpretation of this work is that age-related declines in NAD^+ are not the result of insufficient synthetic capacity or precursor availability, since the rate of new synthesis is unchanged. Instead, it appears that the activity of one or more NAD^+ consumers increases, such that the steady-state concentration falls until consumption flux is brought back in balance with production flux. In cells, we have previously shown that the rate of NAD^+ consumption follows approximately first order kinetics (i.e., consumption flux is directly proportional to NAD^+ concentration) (Liu L, 2018). Thus, we would speculate that the change in consumer activity is likely to be proportional to the change in steady-state NAD^+ concentration – a 2-fold increase in consumption would be balanced by a ~ 50% decrease in steady state to restore flux to its previous level. However, it is not known for certain whether the approximation of first order kinetics holds up *in vivo* or over the course of aging. We also cannot yet say with confidence which NAD^+ consumers are activated with age. The two leading candidates from the literature are CD38 (more active due to inflammatory changes) and PARP1 (activated by DNA damage). However, many NAD^+

consuming enzymes remain poorly characterized *in vivo*. For example, the activities of most mono-ADP-ribosyltransferases have been difficult to study until recently due to the lack of reagents that could detect the mono ADP-ribosyl modification on proteins, and SARM1 has been the subject of intense scrutiny within axons but its roles in other tissues remain virtually unexplored. Importantly, increased activity of any one NAD^+ consumer is expected to correspondingly decrease flux through other consumers by limiting the steady-state NAD^+ concentration. Such competition has previously been described for CD38 (Aksoy P, 2006) and PARP1 (Bai P, 2011), each of which can limit the activity of sirtuins. Therefore, a high priority moving forward is to understand in more detail how the activities of individual NAD^+ consuming enzymes change across the lifespan.

Importantly, while we find that basal rates of NAD^+ synthesis do not change appreciably with age, we do not exclude the possibility that the *capacity* for NAD^+ biosynthesis is diminished. This could become an important limitation under conditions of stress such as DNA damage that drives acute consumption of NAD^+. Moreover, it may be the case that even the basal activity of some NAD^+ biosynthetic enzymes decrease slightly with age, but that the decrease in steady-state NAD^+ concentration relieves feedback inhibition to restore normal flux. Indeed, NAMPT is well known to be subject to feedback inhibition by NAD^+ (Dietrich LS, 1968), and the mild phenotypes of heterozygous animals (Revollo JR, 2007) suggest that its capacity is well in excess of what is used under basal conditions.

Decreased NAD^+ consumption in animals subjected to CR can explain the restoration of NAD^+ concentration in aged liver and WAT, and is in line with expectations of decreased inflammation and DNA damage (Spindler, 2010). However, it is contrary to the view that CR boosts NAD^+ levels via increasing synthesis and thereby driving NAD^+-dependent sirtuins (J. Song, 2014; M. Fulco, 2008; X. Wei, 2020). In fact, despite the lower rates of turnover in animals subjected to CR, we did not observe restoration of tissue NAD^+ concentrations in muscle or kidney, and only detected clear increases in liver and WAT. Thus, CR may intrinsically decrease synthesis in addition to its effects on consumption of NAD^+, either by sensitizing feedback inhibition, or as a consequence of altered metabolism – for example, due to limited production of phosphoribosylpyrophosphate, a product of the pentose phosphate pathway that is required for nucleotide synthesis (Lane, 2015). Mitochondrial NAD^+ labeling patterns tended to closely follow those of bulk tissue, albeit with 10–20% less total labeling as compared to the parent tissue under any given condition. This is consistent with our previous observation that intact NAD^+ can enter the mitochondria, and suggests that the normal turnover of the mitochondrial NAD^+ pool is only modestly slower than that measured for total tissue, despite the fact that mitochondria can retain NAD^+ for some time after depletion of the nuclear and cytosolic pools (Yang H, 2007).

Our findings also have interesting implications for the concept of NAD^+ supplementation. If synthesis rates were impaired with age, then restoring NAD^+ production with supplements such as nicotinamide riboside or mononucleotide, or pharmacological strategies such as NAMPT activation (Gardell SJ, 2019), would simply be restoring normal “youthful” physiology. However, our data suggest that such strategies

would act by boosting synthesis rates beyond normal in the face of increased consumption. This may alleviate the NAD^+ shortage for enzymes such as sirtuins that are proposed to have beneficial effects during aging and to be vulnerable to competition from other consumers. However, it also increases NAD^+ availability to any enzymes that might be hyperactivated with age. The consequences of chronically driving more activation of PARPs or CD38 are not entirely clear, but may need to be considered. On an optimistic note, the worst consequence of PARP1 hyperactivation may well be NAD^+ depletion (Scheibye-Knudsen M, 2014), which is clearly not an issue if the excess activity is driven by NAD^+ oversupply. Determining NAD^+ turnover rates and flux through specific consumer pathways in animals with artificially elevated tissue NAD^+ concentrations will be of great interest in future studies to understand the consequences of supplementation.

In summary, we provide the most comprehensive view of *in vivo* NAD^+ metabolism to date, and the first direct measurements of age-related changes in NAD^+ turnover. Our findings suggest that in most tissues, increased consumption is the primary driver of modest declines in steady-state NAD^+ concentrations with age, whereas synthesis flux is maintained. Importantly, there may be significant heterogeneity between cells types and even among similar cells within a given tissue (e.g., due to local DNA damage or inflammatory foci) that are not resolved with our current methodology. In addition, impaired NAD^+ synthesis has been implicated in the aging of specific cell types, including loss of tryptophan-dependent synthesis in macrophages (Minhas PS, 2019), loss of NMNAT-2 dependent synthesis in aged oocytes (Wu X, 2019), and diminished delivery of circulating NAMPT to the aging hypothalamus and peripheral tissues (Yoshida M, 2019). NAD^+ biosynthesis also drives developmental and reproductive processes (Crook M, 2014; Ear PH, 2019; McReynolds MR, 2017; Wang W, 2015) that are beyond the scope of the present study. Therefore, our data provide a framework for studying systemic changes in NAD^+ metabolism with age, but many details remain to be elucidated, including the roles of specific NAD^+ consuming enzymes, the dynamics of NAD^+ at the level of individual cells and organelles, and metabolic adaptation to acute and chronic stress. The relationships between NAD^+ metabolism and aging remain a subject of great interest, given the likelihood of being able to target this pathway safely in humans and promising data on age-related degenerative conditions in rodent models.

Method Details

Animal Use and Care

All animal procedures were conducted at the University of Pennsylvania and approved by the Institutional Animal Care and Use Committee. C57BL/6J.Nia mice were obtained from the National Institute on Aging Rodent Colony at 3 months (young) and 25 months (old) and acclimatized in the animal facility with *ad libitum* access to laboratory diet 5010 and water on 12h light: dark cycle (7AM- 7PM) for 2-4 weeks. Catheter was surgically implanted in the right jugular vein of the mouse and infusion with isotopically labeled tracer carried out mostly within a week. Single-housed aged *ad libitum* fed and 40% caloric restricted C57BL/6J.Nia mice (21-23 mo) were procured from National Institute on Aging Rodent Colony

and maintained on NIH-31 and NIH-31 fortified diet, respectively for two months prior to use. CR mice were fed a 3g pellet everyday between 8-10 am. Three month old C57BL/6J.Nia mice were single-housed and fed *ad libitum* with NIH-31 for one month prior to catheterization and used as young controls for CR mice.

Intravenous Infusion of Mice

Isotope labeled NAD precursors, [2,4,5,6-^{2}H]-NAM and [U-^{13}C]-Trp (Cambridge Isotope Laboratories, Tewksbury, MA), were infused in young and aged mice for 2-25 hours to achieve steady state NAD labeling from labeled precursors in different tissues (Liu L, 2018). A tether and swivel system (Instech Laboratories, Plymouth Meeting, PA) was used for infusions to provide free movement of mouse in the cage with bedding materials and access to food and hydrogel (Clear H2O, Portland, ME). Infusion conditions in the various experiments are as follows: (1) 50mM [U-^{13}C]-Trp dissolved in saline was infused for 15hr based on their lean mass (1mL per 20 g lean mass per minute) starting at ZT0-2 (2) 4mM [2,4,5,6-^{2}H]-NAM in saline was infused for 2hr, 8hr or 24hr at a constant rate of 1mL per 20 g body weight per minute starting at ZT14-17 (3) Mice in the CR experiment were infused with 4mM [2,4,5,6-^{2}H]-NAM for 12hr starting from ZT23-ZT1 at a constant rate of 1mL per 20 g lean mass (4) In the FK866 experiment, mice were injected with vehicle (45% Propylene glycol, 5% Tween 80, 50% water) or 50 mg/kg FK866 (Selleck Chemicals, Houston, Tx) once every 8hr from ZT14, and infused after 1hr with 4mM [2,4,5,6-^{2}H]-NAM at 1mL per 20 g body weight per minute rate for 23hr.

Blood samples (~20uL) were collected via tail bleeding using microvette blood collection tubes (Sarstedt, Cat. # 16.440.100) and centrifuged at 16,000 g for 15 minutes at 4°C to isolate serum. At the end of the infusion period, mice were euthanized by cervical dislocation and tissues were quickly dissected and clamped in liquid nitrogen. Serum and tissues samples were kept at -80°C before metabolite extraction for mass spectrometry analysis.

Metabolite Extraction from Serum and Tissues

Serum was thawed on ice before adding either -80°C 100% methanol or -80°C 80:20 methanol:water with a volume of 13.5mL solvent per 1mL serum, vortexed, incubated on dry ice for 10 minutes, and centrifuged at 16,000 g for 20 minutes, with the supernatant used for LC-MS analysis. Frozen tissues were weighed, ground with a liquid nitrogen in a cryomill (Retsch) at 25 Hz for 45 seconds, before extracting tissues with 40:40:20 acetonitrile:methanol:water or 40:40:20 acetonitrile:methanol:water with 0.1M formic acid with a volume of 40mL solvent per 1mg of tissue, vortexed for 15 seconds, and incubated on ice for 10 minutes. The samples extracted with formic acid were neutralized with 15% NH4HCO3 as described previously (Lu W, 2018). Tissue samples were then centrifuged at 16,000 g for 30 minutes. The tissue supernatants were transferred to new Eppendorf tubes and then centrifuged again at 16,000 g for 25 minutes to remove and residual debris before analysis.

Eyes were enucleated and transferred to a 35 mm petri dish containing sterile PBS. The posterior half of the eye was trimmed of fat, muscle, and separated from the optic nerve. The anterior half of the eye, including the lens, was removed, and the retina was gently separated from the RPE using fine forceps. The separated retina and eye cup (RPE, choroid, and sclera complex) were dabbed with Kim wipes to remove moisture and snap frozen in microcentrifuge tubes in liquid nitrogen, then stored at -80 °C. The retina and eye cup were ground with a liquid nitrogen in a cryomill (Retsch) at 25 Hz for 45 seconds, before extracting with -80°C 80:20 methanol:water with a volume of 40mL solvent per mg retina or eye cup, vortexed, incubated on dry ice for 10 minutes, and centrifuged at 16,000 g for 20 minutes, with the supernatant used for LC-MS analysis.

Immune Cell Sorting and Metabolite Extraction

Metabolites were extracted from sorted immune cell subpopulations from spleen. Briefly, half of the spleen was smashed and passed through a 70µm strainer. After a cold PBS (Corning #21-031-CV) wash and centrifugation, pellets were resuspended in 1.5ml of Ammonium-Chloride-Potassium buffer (Gibco #A10492-01) for 3min at room temperature. Lysis was blocked by dilution in 30ml of cold PBS. Single cell suspensions were stained with 1µl of each antibody (CD45-APC (30-F11), CD11b PeCy7 (M1/70), CD3 BV510 (17A2) B220 Pe (RA3-6B2) from EBiosciences) for 1.10^6 cells in 100µl of PBS at 4°C protected from light for 30min. After staining, cells were washed once and resuspended in PBS containing 1% of deactivated FBS (Thermofisher sci. #10082147). Sorting was performed on a BD FACSAria Fusion cell sorter. Sorted cells were centrifuged and resuspended in 40:40:20 acetonitrile:methanol:water supplemented with 0.1M formic acid and neutralized with 15% NH4HCO3.

Extraction of Mitochondrial Metabolites

Mitochondria was isolated from fresh tissues as reported previously (Frederick, 2015). Tissue samples were minced in ice-cold mitochondrial isolation buffer (210mM Mannitol, 70mM Sucrose, 10mM HEPES, 1mM EGTA, pH 7.4 with 0.25% fatty acid free bovine serum albumin), and homogenized with Potter Elvehjem homogenizer for 6-10 passes at 150 rpm. The homogenate was centrifuged at 750g for 5 min, and pellet was washed twice at 5000g for 20 min at 4°C. Isolated mitochondria was resuspended in mitochondrial isolation buffer to measure protein concentration and citrate synthase assay. Pelleted mitochondria was extracted using 40:40:20 acetonitrile:methanol:water with 0.1M formic acid. The extract was neutralized with 15% NH4HCO3.

Metabolite Measurement

Extracts were analyzed within 24 hours by liquid chromatography coupled to a mass spectrometer (LC-MS). The LC–MS method involved hydrophilic interaction chromatography (HILIC) coupled to the Q Exactive PLUS mass spectrometer (Thermo Scientific) (Wang L, 2019). The LC separation was performed on a XBridge BEH Amide column (150 mm 3 2.1 mm, 2.5 mm particle size, Waters, Milford, MA). Solvent A is 95%: 5% H2O: acetonitrile with 20 mM ammonium bicarbonate, and solvent B is acetonitrile. The gradient was 0 min, 85% B; 2 min, 85% B; 3 min, 80% B; 5 min, 80% B; 6 min, 75% B; 7 min, 75% B; 8 min,

70% B; 9 min, 70% B; 10 min, 50% B; 12 min, 50% B; 13 min, 25% B; 16 min, 25% B; 18 min, 0% B; 23 min, 0% B; 24 min, 85% B; 30 min, 85% B. Other LC parameters are: flow rate 150 ml/min, column temperature 25°C, injection volume 10 mL and autosampler temperature was 5°C. The mass spectrometer was operated in both negative and positive ion mode for the detection of metabolites. Other MS parameters are: resolution of 140,000 at m/z 200, automatic gain control (AGC) target at 3e6, maximum injection time of 30 ms and scan range of m/z 75-1000. Raw LC/MS data were converted to mzXML format using the command line "msconvert" utility (Adusumilli and Mallick, 2017). Data were analyzed via the MAVEN software, and all isotope labeling patterns were corrected for natural ^{13}C abundance using AccuCor (Su, 2017).

Quantification And Statistical Analysis

Quantification of NAD$^{\pm}$ Fluxes *In Vivo*

We infused [U-$^{13}C_{11}$] Trp and [2,4,5,6-$^{2}H_4$] NAM separately to mice to determine fluxes. [U-$^{13}C_{11}$] Trp (Trp_{11}) resulted in NAD_6 (NAD M+6 with all carbons on the nicotinamide part labeled) and then $NAM_{Tissue,6}$. $NAM_{Tissue,6}$ was then exchanged between tissues and circulation ($NAM_{Serum,6}$) before being taken by tissues to make NAD. NAD_3 was made directly from NAM_4 (one deuteron of NAM_4 becomes the redox-active deuteron of NAD and thus is quickly lost). Breakdown of NAD_3 yields NAM_3.

In each organ, as shown in Figure 3, 4 NAD metabolic fluxes are calculated assuming metabolic steady state in each tissue: is NAD *de novo* synthesis flux from tryptophan, is the flux of NAM being taken up from serum, is NAD synthesis flux from tissue nicotinamide (NAM). At metabolic steady state, the NAD and nicotinamide concentrations in tissue stay constant. Therefore, the mass balance suggests the corresponding breakdown (NAD à NAM) and excretion (tissue NAM à circulation) fluxes are fully determined by the production fluxes above, and thus are not included as separate variables in the model. The following set of differential equations are used to calculate the tissue NAD and NAM labeling patterns at each time point.

$$\begin{cases} \frac{dNAD_0}{dt} = \frac{[f_1(Trp_0 - NAD_0) + f_3(NAM_{Tissue_0} - NAD_0)]}{c_{NAD}} \\ \frac{dNAD_3}{dt} = \frac{[f_1(-NAD_3) + f_3(NAM_{Tissue_3} + NAM_{Tissue_4} - NAD_3)]}{c_{NAD}} \\ \frac{dNAD_6}{dt} = \frac{[f_1(Trp_{11} - NAD_6) + f_3(NAM_{Tissue_6} - NAD_6)]}{c_{NAD}} \\ \frac{dNAM_{Tissue0}}{dt} = \frac{[(f_1+f_3)(NAD_0 - NAM_{Tissue0}) + f_2(NAM_{Serum_0} - NAM_{Tissue_0})]}{c_{NAM}} \\ \frac{dNAM_{Tissue3}}{dt} = \frac{[(f_1+f_3)(NAD_3 - NAM_{Tissue3}) + f_2(NAM_{Serum_3} - NAM_{Tissue_3})]}{c_{NAM}} \\ \frac{dNAM_{Tissue4}}{dt} = \frac{[(f_1+f_3)(-NAM_{Tissue4}) + f_2(NAM_{Serum_4} - NAM_{Tissue_4})]}{c_{NAM}} \\ \frac{dNAM_{Tissue6}}{dt} = \frac{[(f_1+f_3)(NAD_6 - NAM_{Tissue6}) + f_2(NAM_{Serum_6} - NAM_{Tissue_6})]}{c_{NAM}} \end{cases} \quad \text{(Figure 3)}$$

In the equations, NAD_i represent the labeling fraction of mass isotopomer M+i of tissue NAD. $NAM_{Tissue\ i}$ and $NAM_{Serum\ i}$ represent the labeling fraction of tissue NAM and serum NAM M+i, respectively. Trp_{11} represents the labeling fraction of serum tryptophan. c_{NAD} and c_{NAM} are tissue concentrations of NAD(H) and NAM, respectively (in nmol/gram tissue weight).

Tryptophan reached steady state in serum within 30 min, therefore Trp_{11} was treated as constants (59% and 60% in young and old animals, respectively). Serum NAM labeling changes as a function of time. In our differential equations, we did not simulate the serum NAM labeling. Instead, the serum NAM labeling was measured experimentally at a few time points, and the empirical labeling kinetics was obtained through polynomial interpolation. At t=0, NAD_{M+0}, NAM_{M+0} are 1, while all other fractions are 0. For any given set of the three fluxes, the dynamic labeling patterns can be calculated from the differential equations. The calculated values were then compared to the measured labeling patterns of tissue NAM and NAD (2 h, 8 h, 24 h during [2,4,5,6-^{2}H] NAM infusion, 15 h after [U-^{13}C] Trp infusion). The tissue concentration of NAM and NAD were also measured. The best estimated flux set is achieved by minimizing the deviation between the calculated labeling patterns and the measured ones. The deviation in each labeled fraction is weighted by the reciprocal of the standard deviation of the replicate experimental labeling measurements. The numerical simulation of the differential equations was performed in R with the deSolve package and the optimization was performed with DEoptim package. 95% confidence intervals of the NAD turnover rates were estimated by chi-square test (cutoff $\chi^2_{0.05}(df=1)=3.84$) (MR Antoniewicz, 2006).

Statistical Analysis

Data are displayed as mean ± SEM. In figures, asterisks denote statistical significance as calculated by a two-tailed unpaired Student's t-test (§, $p < 0.1$, *, $p < 0.05$; **, $p < 0.01$; ***, $p<0.001$). This test is appropriate for determining whether the means of two populations are equal. Data were not tested for the assumptions of normality and equal variance across groups. Exponential curve fitting was used to test whether data followed an exponential decay pattern. Statistical parameters are reported in the Figures and Figure Legends. $P<0.05$ was considered statistically significant. N represents the number of replicates.

Declarations

Acknowledgments:

This work was funded and supported by both the Howard Hughes Medical Institute and Burroughs Wellcome Fund via the PDEP and Hanna H. Gray Fellow Programs awarded to MRM; Crohn's and Colitis Career Development Award to KC; NIH grants CA211437 to WL, DP1DK113643 to JDR, R01DK098656 and R01AG043483 to JAB. Furthermore, we acknowledged CINJ Cancer Center Support Grant, Rutgers Cancer Institute of New Jersey Metabolomics Shared Resource, supported, in part, with funding from NCI-CCSG P30CA072720-5923.

Author Contributions:

MRM, KC, JDR, and JAB conceived the project and designed experiments. MRM and KC performed and analyzed most experiments. MRM and XS conducted the flux analysis. MRM, KC, EC, CJ, YS, LC, HCD, SM, YRB, QC, XJ, FS, and PB performed specific *in vivo* experiments and analyses. MRM and JAB wrote the manuscript. KC and JDR edited the manuscript, and all authors provided input.

Competing Interest Statement:

J.A.B. and S.M. declare that they have intellectual property related to using NAD^+ precursors in liver injury. J.D.R. declares that he is a co-founder of Toran Therapeutics. The remaining authors have nothing to declare.

References

Adusumilli, R., and Mallick, P. (2017). Data Conversion with ProteoWizard msConvert. Methods Mol Biol *1550*, 339-368.

Aksoy P, E.C., White TA, Thompson M, Soares S, Benech JC, Chini EN. (2006). Regulation of SIRT 1 mediated NAD dependent deacetylation: a novel role for the multifunctional enzyme CD38. Biochem Biophys Res Commun *349*, 353-359.

Amici SA, Y.N., Narvaez-Miranda J, Jablonski KA, Arcos J, Rosas L, Papenfuss TL, Torrelles JB, Jarjour WN, Guerau-de-Arellano M (2018). CD38 Is Robustly Induced in Human Macrophages and Monocytes in Inflammatory Conditions. Front Immunol *9*, 1593.

Anderson, R.M., and Weindruch, R. (2012). The caloric restriction paradigm: implications for healthy human aging. Am J Hum Biol *24*, 101-106.

Bai P, C.C., Oudart H, Brunyánszki A, Cen Y, Thomas C, Yamamoto H, Huber A, Kiss B, Houtkooper RH, Schoonjans K, Schreiber V, Sauve AA, Menissier-de Murcia J, Auwerx J. (2011). PARP-1 inhibition increases mitochondrial metabolism through SIRT1 activation. Cell Metab *13*, 461-468.

Behr A, T.H., Gholson RK. (1981). Apparent pyridine nucleotide synthesis in mitochondria: an artifact of NMN and NAD glycohydrolase activity? Biochem Biophys Res Commun *101*, 767-774.

Braidy N, G.G., Mansour H, Chan-Ling T, Poljak A, Grant R. (2011). Age related changes in NAD+ metabolism oxidative stress and Sirt1 activity in wistar rats. PLoS One *6*, e19194.

Brand, M.D. (1997). Regulation Analysis of Energy Metabolism. J Exp Biol *200*, 193-202.

C.A. Sims, Y.G., S. Mukherjee, K. Singh, P. Botolin, A. Davila Jr., and J.A. Baur (2018). Nicotinamide Mononucleotide Preserves Mitochondrial Function and Increases Survival in Hemorrhagic Shock. JCI Insight *3*, e120182.

Camacho-Pereira, J., Tarrago, M.G., Chini, C.C.S., Nin, V., Escande, C., Warner, G.M., Puranik, A.S., Schoon, R.A., Galina, A., and Chini, E.N. (2016). CD38 Dictates Age-Related NAD Decline and Mitochondrial Dysfunction through an SIRT3-Dependent Mechanism. Cell Metab *23*, 1127–1139.

Chalkiadaki, A., and Guarente, L. (2012). Sirtuins mediate mammalian metabolic responses to nutrient availability. Nat Rev Endocrinol *8*, 287-296.

Chen D, B.J., Easlon E, Lin SJ, Cheng HL, Alt FW, Guarente L. (2008). Tissue-specific regulation of SIRT1 by calorie restriction. Genes Dev *22*, 1753-1757.

Chen, D., Steele, A.D., Lindquist, S., and Guarente, L. (2005). Increase in activity during calorie restriction requires Sirt1. Science *310*, 1641.

Chini C, H.K., Warner GM, Tarragó MG, Peclat TR, Tchkonia T, Kirkland JL, Chini E. (2019). The NADase CD38 is induced by factors secreted from senescent cells providing a potential link between senescence and age-related cellular NAD+ decline. Biochem Biophys Res Commun *513*, 486-493.

Chini, C., Tarrago, M. & Chini, E. (2017). NAD and the aging process: Role in life, death and everything in between. Mol Cell Endocrinol *445*, 62-74.

Clement J, W.M., Poljak A, Sachdev P, Braidy N (2019). The Plasma NAD+ Metabolome Is Dysregulated in "Normal" Aging. Rejuvenation Res *22*, 121-130.

Crook M, M.M., Wang W, Hanna-Rose W. (2014). An NAD(+) biosynthetic pathway enzyme functions cell non-autonomously in C. elegans development. Dev Dyn *243*, 965-976.

Davila A, L.L., Chellappa K, Redpath P, Nakamaru-Ogiso E, Paolella LM, Zhang Z, Migaud ME, Rabinowitz JD, Baur JA. (2018). Nicotinamide adenine dinucleotide is transported into mammalian mitochondria. Elife *pii: e33246*.

Dietrich LS, M.O., Powanda M. (1968). NAD synthesis in animal tissues. J Vitaminol (Kyoto) *14*, 123-129.

E.F. Fang, M.S.-K., L.E. Brace, H. Kassahun, T. SenGupta, H. Nilsen, J.R. Mitchell, D.L. Croteau and V.A. Bohr (2014). Defective Mitophagy in XPA via PARP-1 Hyperactivation and NAD+/SIRT1 Reduction. Cell *157*, 882-896.

Ear PH, C.A., Gumusoglu SB, Schmidt MS, Vogeler S, Malicoat J, Kadel J, Moore MM, Migaud ME, Stevens HE, Brenner C. (2019). Maternal Nicotinamide Riboside Enhances Postpartum Weight Loss, Juvenile Offspring Development, and Neurogenesis of Adult Offspring. Cell Rep *26*, 969-983.

Frederick, D.W., Davis, J.G., , Dávila, A.J., Agarwal, B., Michan, S., Puchowicz, M.A., Nakamaru-Ogiso||, E. and J. A. Baur (2015). Increasing NAD Synthesis in Muscle via Nicotinamide Phosphoribosyltransferase Is Not Sufficient to Promote Oxidative Metabolism. JBC *290*,, 1546-1558.

Frederick DW, L.E., Liu L, Davila A Jr, Chellappa K, Silverman IM, Quinn WJ 3rd, Gosai SJ, Tichy ED, Davis JG, Mourkioti F, Gregory BD, Dellinger RW, Redpath P, Migaud ME, Nakamaru-Ogiso E, Rabinowitz JD, Khurana TS, Baur JA. (2016). Loss of NAD Homeostasis Leads to Progressive and Reversible Degeneration of Skeletal Muscle. Cell Metab *24*, 269-282.

Gardell SJ, H.M., Khan A, Dispagna M, Hampton Sessions E, Falter R, Kapoor N, Brooks J, Culver J, Petucci C, Ma CT, Cohen SE, Tanaka J, Burgos ES, Hirschi JS, Smith SR, Sergienko E, Pinkerton AB. (2019). Boosting NAD+ with a small molecule that activates NAMPT. Nat Commun *10*, 3241.

Gomes, A.P., Price, N. L., Ling, A. J. Y., Moslehi, J. J., Montgomery, M. K., Rajman, L., White, J.P., Teodoro, J.S., Wrann, C.D., Hubbard, B.P., Mercken, E.M., Palmeria, C.M., deCabo, R., Rolo, A.P., Turner, N., Bell, E.L., and Sinclair, D. A. (2013). Declining NAD+ induces a pseudohypoxic state disrupting nuclear103 mitochondrial communication during aging. Cell *155*, 1624-1638.

Guan Y, W.S., Huang XZ, Xie QH, Xu YY, Shang D, Hao CM (2017). Nicotinamide mononucleotide, an NAD+ precursor, rescues age-associated susceptibility to AKI in a sirtuin 1-dependent manner. J Am Soc Nephrol *28*, 2337-2352.

J. Song, S.K., C. Zhou, S. Zhang, Y. Guan, T. Xu, C. Sheng, P. Wang, C. Miao (2014). Nicotinamide Phosphoribosyltransferase Is Required for the Calorie Restriction-Mediated Improvements in Oxidative Stress, Mitochondrial Biogenesis, and Metabolic Adaptation. J Gerontol A Biol Sci Med Sci *69*, 44-57.

Kang BN, T.K., Deshpande DA, Amrani Y, Panettieri RA, Walseth TF, Kannan MS (2006). Transcriptional regulation of CD38 expression by tumor necrosis factor-alpha in human airway smooth muscle cells: role of NF-kappaB and sensitivity to glucocorticoids. FASEB J *20*, 1000-1002.

Lane, A.N.a.F., T. W.-M. (2015). Regulation of mammalian nucleotide metabolism and biosynthesis. Nucleic Acids Res *43*, 2466–2485.

Liu L, S.X., Quinn WJ, Hui S, Krukenberg K, Frederick DW, Redpath P, Zhan L, Chellappa K, White E, Migaud M, Mitchison TJ, Baur JA, Rabinowitz JD. (2018). Quantitative Analysis of NAD Synthesis-Breakdown Fluxes. Cell Metab *27*, 1067-1080.e1065.

Lu W, W.L., Chen L, Hui S, Rabinowitz JD (2018). Extraction and Quantitation of Nicotinamide Adenine Dinucleotide Redox Cofactors. Antioxid Redox Signal *28*, 167-179.

M. Fulco, Y.C., P. Zhao, E.P. Hoffman, M.W. McBurney, A. A .Sauve, V. Sartorelli (2008). Glucose Restriction Inhibits Skeletal Myoblast Differentiation by Activating SIRT1 Through AMPK-mediated Regulation of Nampt. Dev Cell *14*, 661-673.

Massudi, H., Grant, R., Braidy, N., Guest, J., Farnsworth, B., and Guillemin, G.J. (2012). Age-Associated Changes In Oxidative Stress and NAD+ Metabolism In Human Tissue. PLoS ONE *7*.

Matalonga J, G.E., Bresque M, Escande C, Carbó JM, Kiefer K, Vicente R, León TE, Beceiro S, Pascual-García M, Serret J, Sanjurjo L, Morón-Ros S, Riera A, Paytubi S, Juarez A, Sotillo F, Lindbom L, Caelles C, Sarrias MR, Sancho J, Castrillo A, Chini EN, Valledor AF (2017). The Nuclear Receptor LXR Limits Bacterial Infection of Host Macrophages through a Mechanism that Impacts Cellular NAD Metabolism. Cell Rep *18*, 1241-1255.

Mattison, J.A., Colman, R.J., Beasley, T.M., Allison, D.B., Kemnitz, J.W., Roth, G.S., Ingram, D.K., Weindruch, R., de Cabo, R., and Anderson, R.M. (2017). Caloric restriction improves health and survival of rhesus monkeys. Nat Commun *8*, 14063.

McReynolds MR, C.K., Baur JA. (2020). Age-related NAD+ decline. Exp Gerontol *134*, 110888.

McReynolds MR, W.W., Holleran LM, Hanna-Rose W (2017). Uridine monophosphate synthetase enables eukaryotic de novo NAD+ biosynthesis from quinolinic acid. J Biol Chem *292*, 11147-11153.

Mills, K.F., Yoshida, S., Stein, L.R., Grozio, A., Kubota, S., Sasaki, Y., Redpath, P., Miguad, M.S., Apte, R.S., Uchida, K., Yoshino, J., and Imai, S.I. (2016). Long-Term Administration of Nicotinamide Mononucleotide Mitigates Age-Associated Physiological Decline in Mice. Cell Metabolism *24*, 795–806.

Minhas PS, L.L., Moon PK, Joshi AU, Dove C, Mhatre S, Contrepois K, Wang Q, Lee BA, Coronado M, Bernstein D, Snyder MP, Migaud M, Majeti R, Mochly-Rosen D, Rabinowitz JD, Andreasson KI (2019). Macrophage de novo NAD+ synthesis specifies immune function in aging and inflammation. Nat Immunol *20*, 50-63.

Mouchiroud, L., Houtkooper, R. H., & Auwerx, J. (2013). NAD+ metabolism: a therapeutic target for age-related metabolic disease. Crit Rev Biochem Mol Bio *48*, 397–408.

MR Antoniewicz, J.K., G Stephanopoulos (2006). Determination of confidence intervals of metabolic fluxes estimated from stable isotope measurements. Metab Eng *4*, 324-337.

Musso T, D.S., Franco L, Calosso L, Badolato R, Garbarino G, Dianzani U, Malavasi F (2001). CD38 expression and functional activities are up-regulated by IFN-gamma on human monocytes and monocytic cell lines. J Leukoc Biol *69*, 605-612.

Pittelli M, F.L., Faraco G, Lapucci A, Rapizzi E, Cialdai F, Romano G, Moneti G, Moroni F, Chiarugi A. (2010). Inhibition of nicotinamide phosphoribosyltransferase: cellular bioenergetics reveals a mitochondrial insensitive NAD pool. J Biol Chem *285*, 34106-34114.

Pollak, N., Dölle, C. and Ziegler, M. (2007). The power to reduce: pyridine nucleotides – small molecules with a multitude of functions. Biochem J *402*, 205–218.

Revollo JR, K.A., Mills KF, Satoh A, Wang T, Garten A, Dasgupta B, Sasaki Y, Wolberger C, Townsend RR, Milbrandt J, Kiess W, Imai S. (2007). Nampt/PBEF/Visfatin regulates insulin secretion in beta cells as a systemic NAD biosynthetic enzyme. Cell Metab *6*, 363-375.

Salvatori, I., Valle, C., Ferri, A., and Carri, M.T. (2017). SIRT3 and mitochondrial metabolism in neurodegenerative diseases. Neurochemistry International *109*, 184-192.

Sauve AA, M.C., Lee HC, Schramm VL. (1998). The reaction mechanism for CD38. A single intermediate is responsible for cyclization, hydrolysis, and base-exchange chemistries. Biochemistry *37*, 13239-13249.

Sauve AA, S.V. (2003). Sir2 regulation by nicotinamide results from switching between base exchange and deacetylation chemistry. Biochemistry *42*, 9249-9256.

Scheibye-Knudsen M, M.S., Fang EF, Iyama T, Ward T, Wang J, Dunn CA, Singh N, Veith S, Hasan-Olive MM, Mangerich A, Wilson MA, Mattson MP, Bergersen LH, Cogger VC, Warren A, Le Couteur DG, Moaddel R, Wilson DM, Croteau DL, de Cabo R, Bohr VA. (2014). A high-fat diet and NAD(+) activate Sirt1 to rescue premature aging in cockayne syndrome. Cell Metab *20*, 840-855.

Shibata, K. (2018). Organ Co-Relationship in Tryptophan Metabolism and Factors That Govern the Biosynthesis of Nicotinamide from Tryptophan. J Nutr Sci Vitaminol (Tokyo) *64*, 90-98.

Someya, S., Yu, W., Hallows, W.C., Xu, J., Vann, J.M., Leeuwenburgh, C., Tanokura, M., Denu, J.M., and Prolla, T.A. (2010). Sirt3 mediates reduction of oxidative damage and prevention of age-related hearing loss under caloric restriction. Cell *143*, 802-812.

Song J, K.S., Zhou CC, Zhang SL, Guan YF, Xu TY, Sheng CQ, Wang P, Miao CY. (2014). Nicotinamide phosphoribosyltransferase is required for the calorie restriction-mediated improvements in oxidative stress, mitochondrial biogenesis, and metabolic adaptation. J Gerontol A Biol Sci Med Sci *69*, 44-57.

Spindler, S.R. (2010). Caloric Restriction: From Soup to Nuts. Ageing Res Rev *9*, 324-353.

SR, S. (2010). Caloric restriction: from soup to nuts. Ageing Res Rev *9*, 324-353.

Srivastava, S. (2016). Emerging therapeutic roles for NAD+ metabolism in mitochondrial and age-related disorders. Clin Trans Med *5*, 25.

Stein LR, I.S. (2014). Specific ablation of Nampt in adult neural stem cells recapitulates their functional defects during aging. EMBO J *33*, 1321-1340.

Su, X., Lu, W., Rabinowitz, J. D. (2017). Metabolite spectral accuracy on orbitraps. Anal Chem *89*, 5940-5948.

Tarragó MG, C.C., Kanamori KS, Warner GM, Caride A, de Oliveira GC, Rud M, Samani A, Hein KZ, Huang R, Jurk D, Cho DS, Boslett JJ, Miller JD, Zweier JL, Passos JF, Doles JD, Becherer DJ, Chini EN (2018). A Potent and Specific CD38 Inhibitor Ameliorates Age-Related Metabolic Dysfunction by Reversing Tissue NAD+ Decline. Cell Metab *27*, 1081-1095.

Ubaida-Mohien C, L.A., Gonzalez-Freire M, Tharakan R, Shardell M, Moaddel R, Semba RD, Chia CW, Gorospe M, Sen R, Ferrucci L (2019). Discovery proteomics in aging human skeletal muscle finds change in spliceosome, immunity, proteostasis and mitochondria. Elife *e49874*.

Verdin, E. (2015). NAD+ in aging, metabolism, and neurodegeneration. Science *350*, 1208-1213.

Wang, G., Han,T., Nijhawan, D., Theodoropoulos, P., Naidoo, J., Yadavalli, S., Mizaei, H., Pieper, A.A., Ready, J.M., McKnight, S.L. (2014). P7C3 Neuroprotective Chemicals Function by Activating the Rate-limiting Enzyme in NAD Salvage. Cell *158*, 1324–1334.

Wang L, X.X., Chen L, Yang L, Su X, Rabitz H, Lu W, Rabinowitz JD (2019). Peak Annotation and Verification Engine for Untargeted LC-MS Metabolomics. Anal Chem *91*, 1838-1846.

Wang W, M.M., Goncalves JF, Shu M, Dhondt I, Braeckman BP, Lange SE, Kho K, Detwiler AC, Pacella MJ, Hanna-Rose W. (2015). Comparative Metabolomic Profiling Reveals That Dysregulated Glycolysis Stemming from Lack of Salvage NAD+ Biosynthesis Impairs Reproductive Development in Caenorhabditis elegans. J Biol Chem *290*, 26163-26179.

Wu X, H.F., Zeng J, Han L, Qiu D, Wang H, Ge J, Ying X, Wang Q (2019). NMNAT2-mediated NAD+ generation is essential for quality control of aged oocytes. Aging Cell *8*, e12955.

X. Wei, R.J., G. Wang, S. Hong, L. Song, B. Sun, K. Chen, N. Wang, Q. Wang, X. Luo, J. Yan (2020). Depot-specific regulation of NAD+/SIRTs metabolism identified in adipose tissue of mice in response to high-fat diet feeding or calorie restriction. The Journal of Nutritional Biochemistry *80*, 108377.

Yang H, Y.T., Baur JA, Perez E, Matsui T, Carmona JJ, Lamming DW, Souza-Pinto NC, Bohr VA, Rosenzweig A, de Cabo R, Sauve AA, Sinclair DA. (2007). Nutrient-sensitive mitochondrial NAD+ levels dictate cell survival. Cell *130*, 1095-1107.

Yang, Y., and Sauve, A. A. (2016). NAD+ metabolism: Bioenergetics, signaling and manipulation for therapy. Biochim Biophys Acta *1864*, 1787–1800.

Yoshida M, S.A., Lin JB, Mills KF, Sasaki Y, Rensing N, Wong M, Apte RS, Imai SI. (2019). Extracellular Vesicle-Contained eNAMPT Delays Aging and Extends Lifespan in Mice. Cell Metab *30*, 329-342.

Yoshino J, B.J., Imai SI (2018). NAD+ Intermediates: The Biology and Therapeutic Potential of NMN and NR. Cell Metab *27*, 513-528.

Zhang, H., Ryu, D., Wu, Y., Gariani, K., Wang, X., Luan, P., D'Amico, D., Ropelle, E.R., Lutolf, M.P., Aebersold, R., Schoonjans, K., Menzies, K.J., and Auwerx, J. (2016). NAD+ repletion improves mitochondrial and stem cell function and enhances life span in mice. Science *352*, 1436–1443.

Zhu X, S.W., Wang Y, Jaiswal A, Ju Z, Sheng Q (2017). Nicotinamide adenine dinucleotide replenishment rescues colon degeneration in aged mice. Signal Transduct Target Ther *7*, 17017.

Zhu XH, L.M., Lee BY, Ugurbil K, Chen W (2015). In vivo NAD assay reveals the intracellular NAD contents and redox state in healthy human brain and their age dependences. 112, 2876-2881.

Tables

Table 1. Metabolic flux distributions in young and aged tissues. Highlighted values represent fluxes in the aged mice that significantly improve the fit as compared to assuming no change from the young values. Goodness of fit and significance were evaluated by chi-square test, $\chi^2_{0.05}(df=3) = 7.8$.

Tissue	Young (*f1*)	Aged (*f1*)	Young (*f2*)	Aged (*f2*)	Young (*f3*)	Aged (*f3*)
Liver	32.8	34.9	34.1	46.3	203.1	327.9
Kidney	0.7	0.0	40.0	35.5	68.3	73.7
Quad	0.0	0.0	8.3	6.0	8.2	6.2
BAT	0.0	0.0	8.7	5.8	38.6	46.8
Heart	0.0	0.0	26.3	20.8	40.9	34.6
Spleen	0.4	0.0	96.8	80.2	315.1	809.8
Jejunum	0.0	0.0	90.8	41.2	782.2	1845.7
Brain	0.0	0.0	9.6	7.7	37.9	39.0
Pancreas	0.0	0.0	58.8	37.4	33.1	20.8
gWAT	0.0	0.0	2.3	1.3	9.2	7.3
Ileum	0.0	0.0	76.4	34.9	1203.8	1232.9
PColon	0.0	0.0	40.1	24.5	764.1	685.3

- Fluxes (μmol/g/hr) | Trp→NAD (*f1*) | NAM uptake (*f2*) | NAM→NAD (*f3*)

Figures

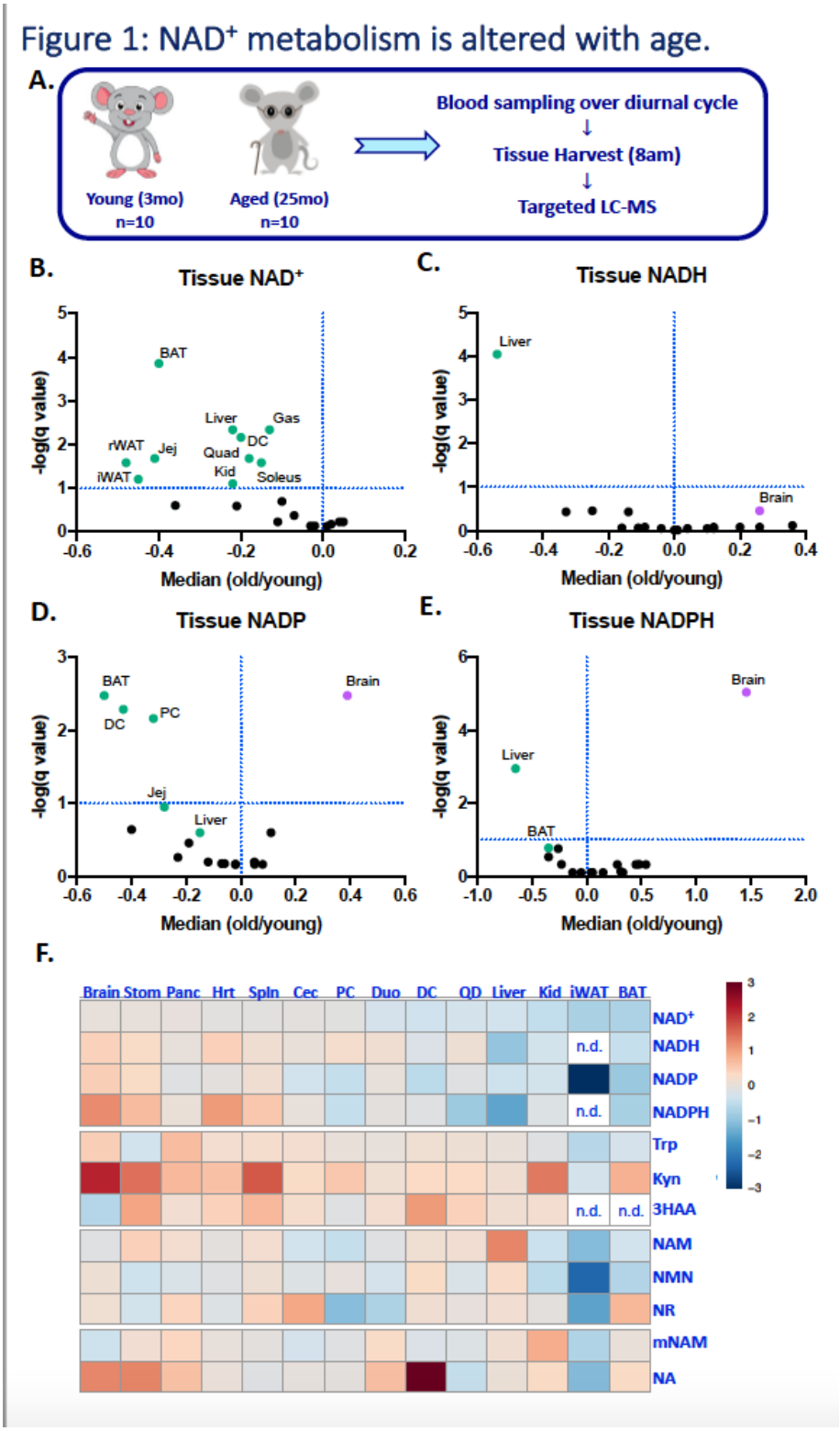

Figure 1

NAD+ metabolism is altered with age. A, schematic for collecting serum and tissue harvesting in young (3mo) and aged (25mo) C57BL/6 mice from NIA aged colony. B-E, Volcano plot representing LC-MS measurements for NAD(H) and NADP(H) across tissues in aged versus young mice. The x-axis represents the median and the y-axis represents adjusted FDR. Colored dots represents tissues that change with age

significantly. F, Heat map representing the whole-body metabolome in aged mice. For each tissue and metabolite, aged are normalized to the median of young, and then log2 transformed.

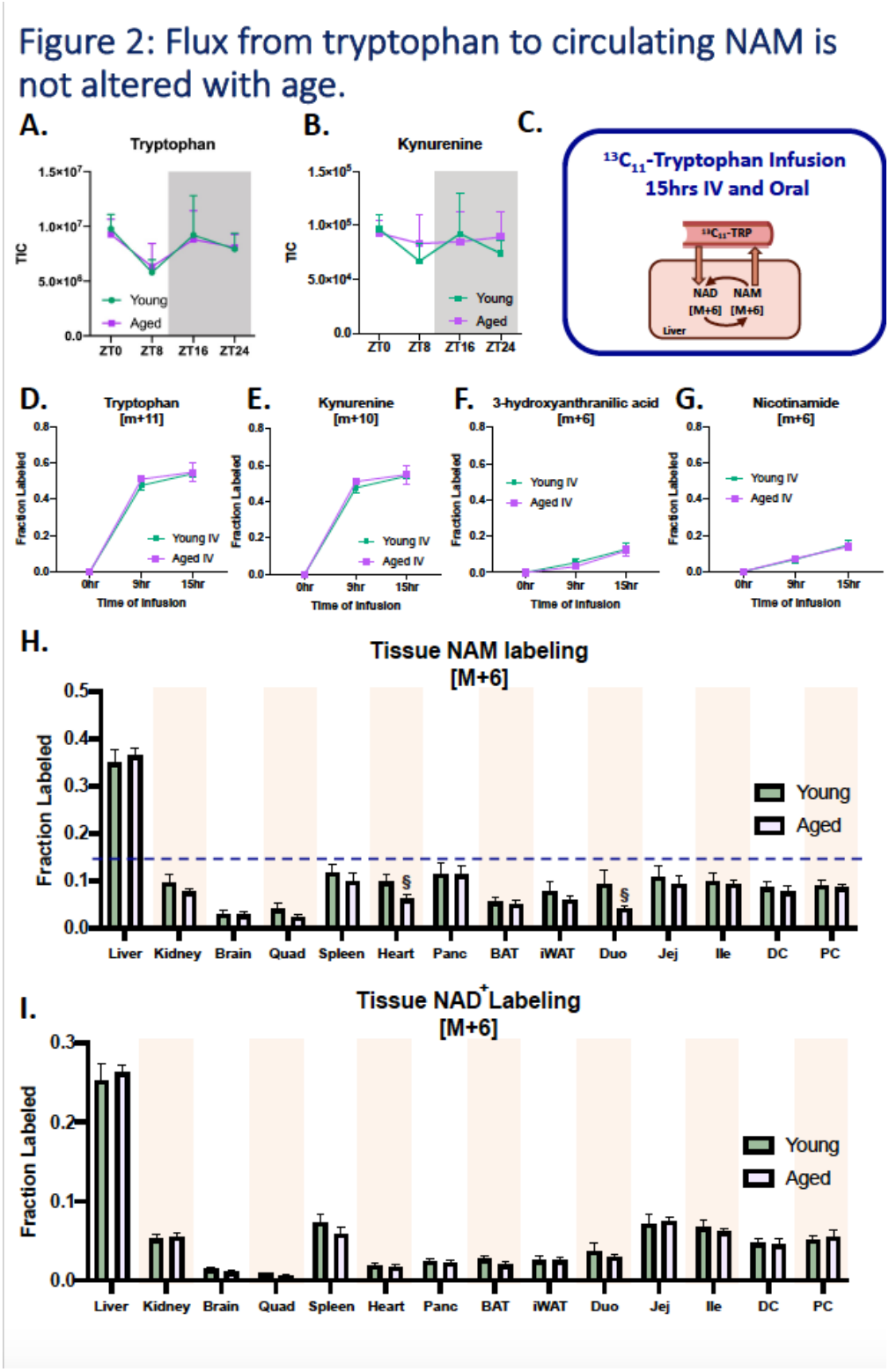

Figure 2

Flux from tryptophan to circulating NAM is not altered with age. A-B, LC-MS measurements of Trp metabolites (Trp and Kyn) in circulation C, Experimental design for infusing universally-labeled-Trp intravenously and orally in young (3mo) and aged (25mo) C57BL/6 mice. D, Fraction Trp labeling over 15

hours. E, Fraction Kyn labeling F, fraction 3HAA labeling, G, fraction NAM labeling from Trp in young and aged mice circulation. H, Tissue NAM labeling from Trp. Dashed line represents serum NAM enrichment highlighting that the liver exceeds serum NAM labeling and all other tissues fall below serum enrichment. I, Tissue NAD+ labeling from Trp. Tissue labeling combines both oral and IV infusion. Young, n=7-8; aged, n=6-9. For all panels, error bars indicate S.E.M. ***, p < 0.001; **, p < 0.01; *, p < 0.05; §, p < 0.1, calculated with Student's t-test.

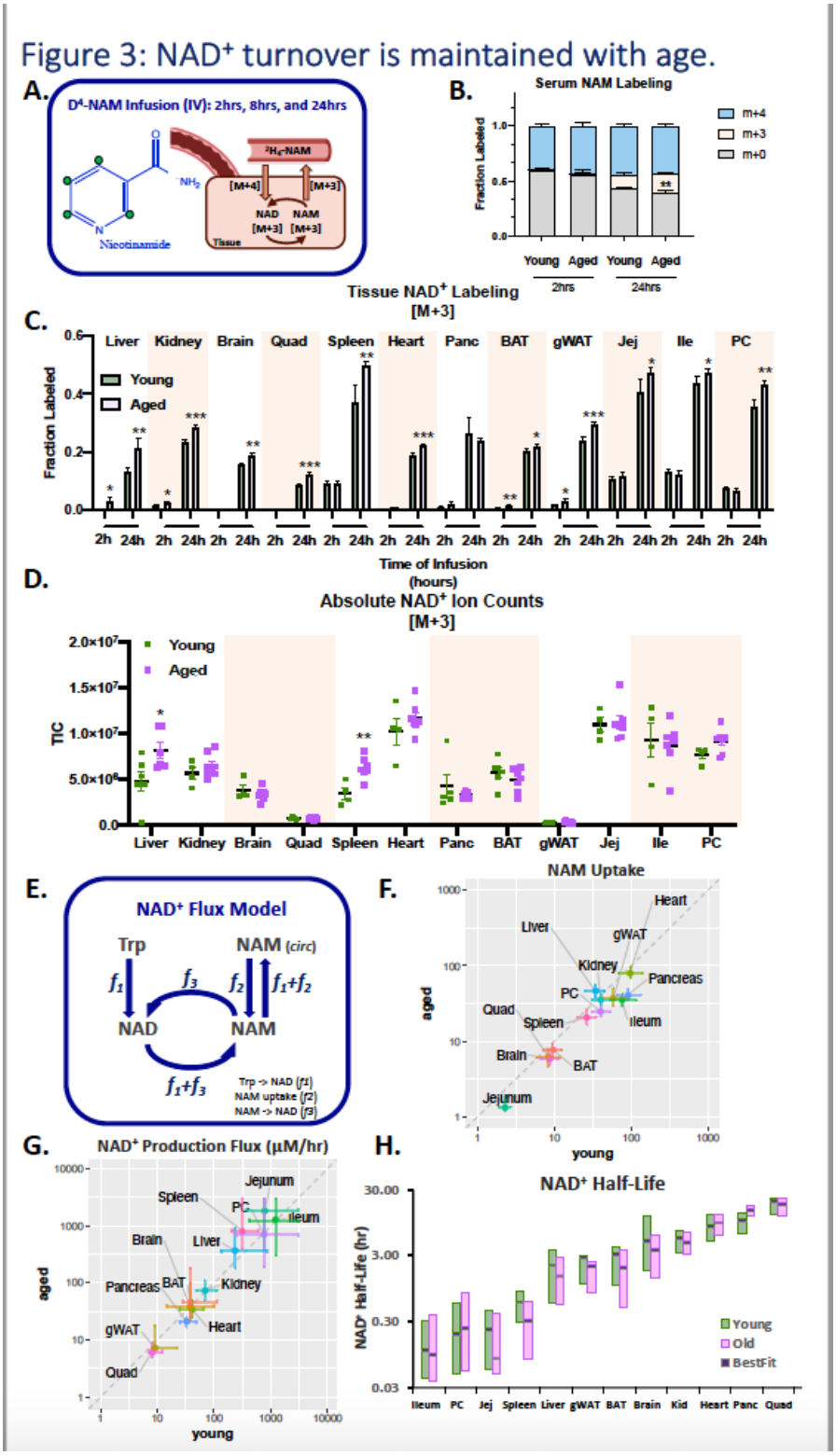

Figure 3

NAD+ turnover is maintained with age. A, Schematic for experimental design for infusing deuterium-labeled-NAM intravenously in young (3mo) and aged (25mo) C57BL/6 mice. B, Fraction circulating NAM labeling over 2hr and 24 hours. C, Tissue NAD+ labeling over 2 and 24 hours in rapid tissues. D, Absolute ion counts for NAD+ M+3 in young and aged mice after 24hr NAM labeling. E, Schematic illustrating model components for NAD+ flux. F, Log-log plot representing NAM uptake in young and aged mice. G, Log-log plot representing NAD+ production fluxes in young and aged tissues. H, NAD+ labeling halftime across tissues in young and aged mice. Young, n=6-9; aged, n=7. For all panels, error bars indicate S.E.M. ***, $p < 0.001$; **, $p < 0.01$; *, $p < 0.05$; §, $p < 0.1$, calculated with Student's t-test.

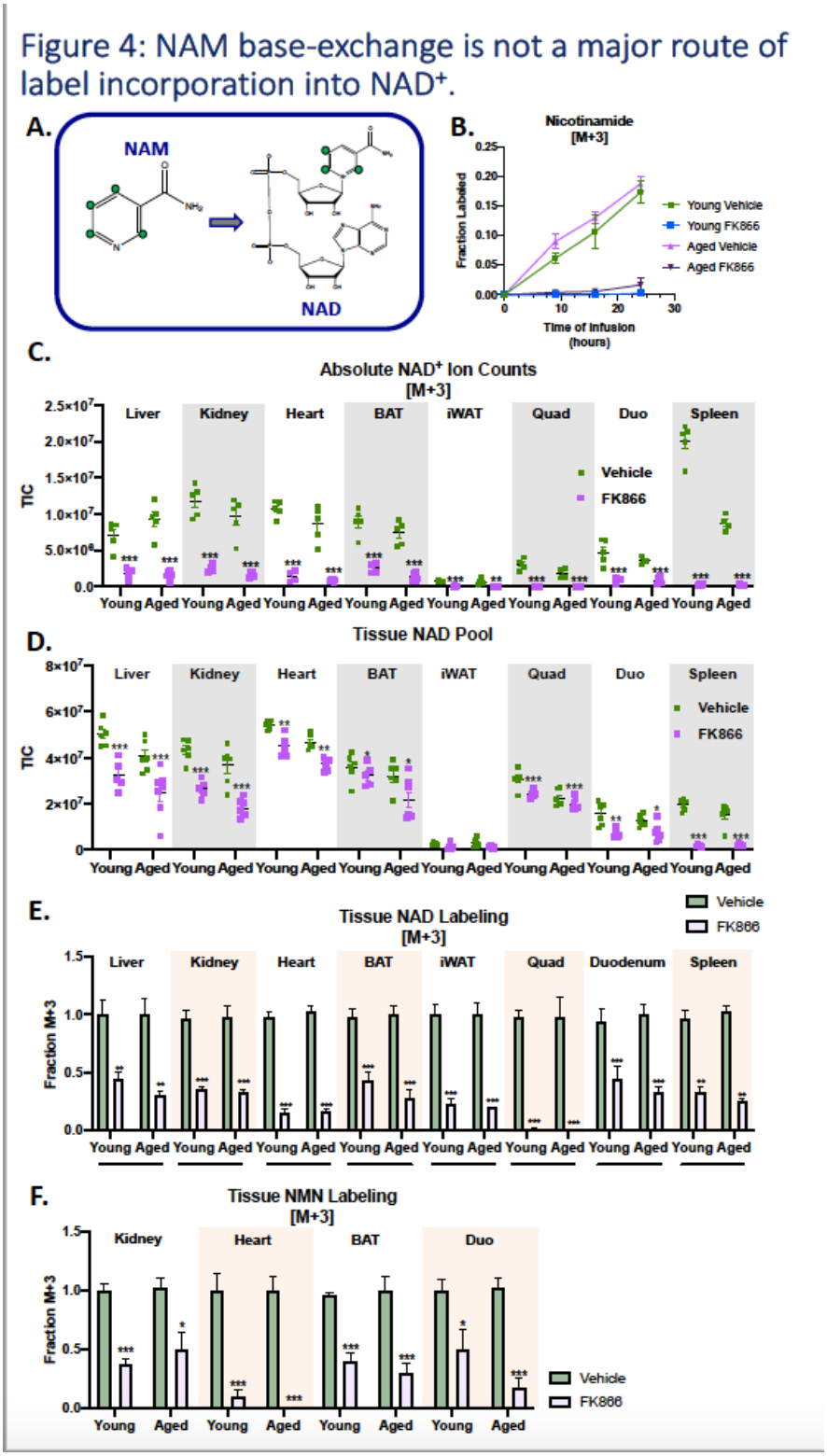

Figure 4

NAM base-exchange is not a major route of label incorporation into NAD+. A, schematic illustrating the potential of NAD consuming enzymes catalyzing a base-exchange reaction, whereby the free NAM replaces the NAM moiety on NAD+. B, Fraction circulating NAM M+3 labeling over 9hrs, 16hrs and 24 hours. C, Absolute ion counts for NAD+ M+3 in young and aged mice treated with Fk866. D, Tissue NAD+ pools in young and aged mice after treatment with FK866. E, Tissue NAD+ turnover at 24hr of NAM

labeling. F, Tissue NMN labeling after 24hrs of infusing with NAM in young and aged mice treated with FK866. For all panels, error bars indicate S.E.M. ***, p < 0.001; **, p < 0.01; *, p < 0.05; §, p < 0.1, calculated with Student's t-test.

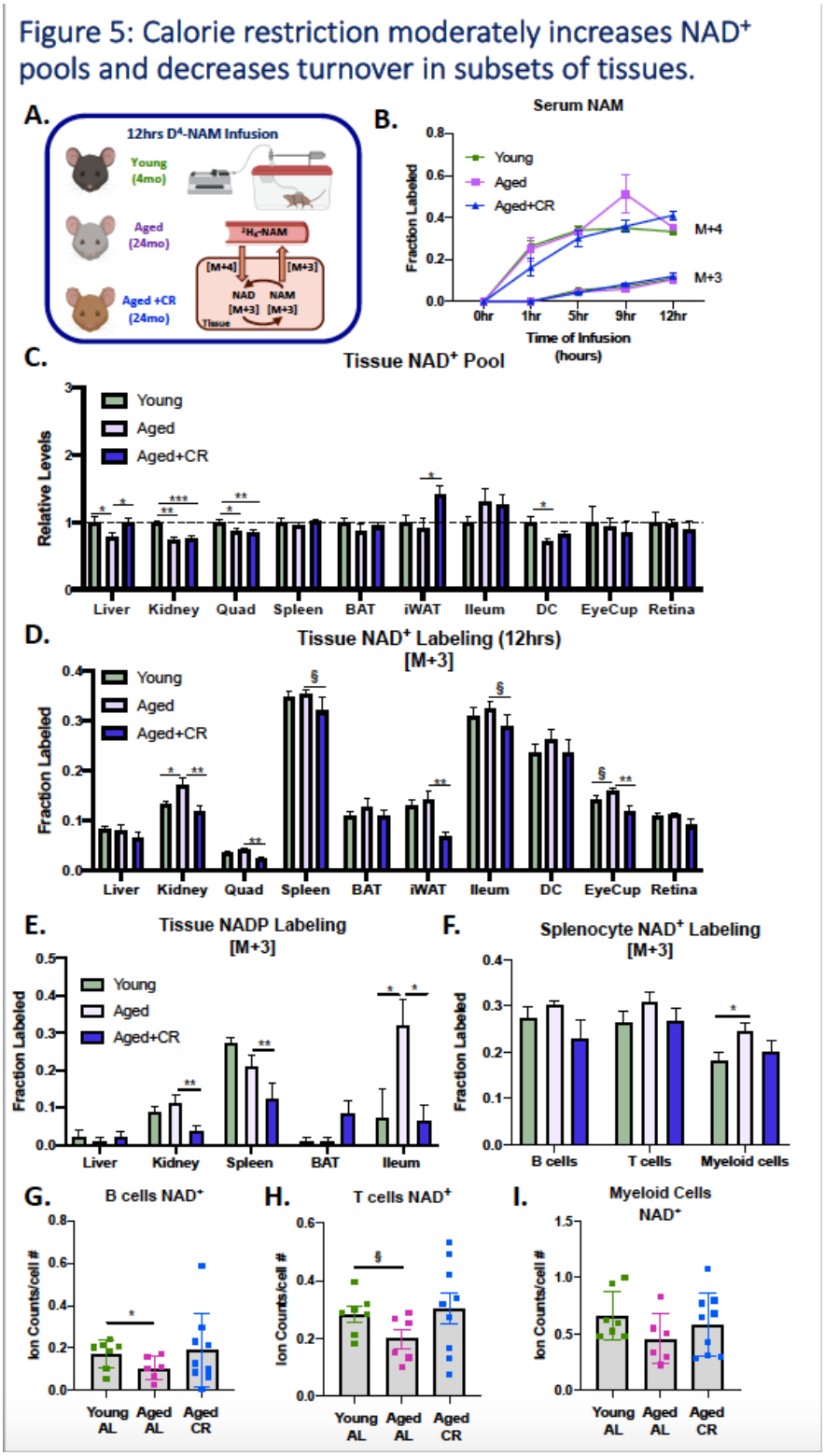

Figure 5

Calorie restriction moderately increase NAD+ pools and decreases turnover in subsets of tissues. A, Schematic for experimental design. B, Fraction circulating NAM labeling over 12 hours in young, aged

and aged +CR mice. C, Tissue NAD+ pools in young, aged and aged +CR mice. D, Tissue NAD+ turnover at 12hrs of NAM labeling. E, Tissue NADP labeling after 12hrs in young, aged and aged +CR mice. F, Splenocyte NAD+ turnover from circulating NAM. G-I, Splenocyte T cells, B cells and myeloid cells NAD+ pools in young, aged and aged +CR mice. Young, n=6; aged, n=6; aged+CR, n=7. For all panels, error bars indicate S.E.M ***, p < 0.001; **, p < 0.01; *, p < 0.05; §, p < 0.1, calculated with Student's t-test.

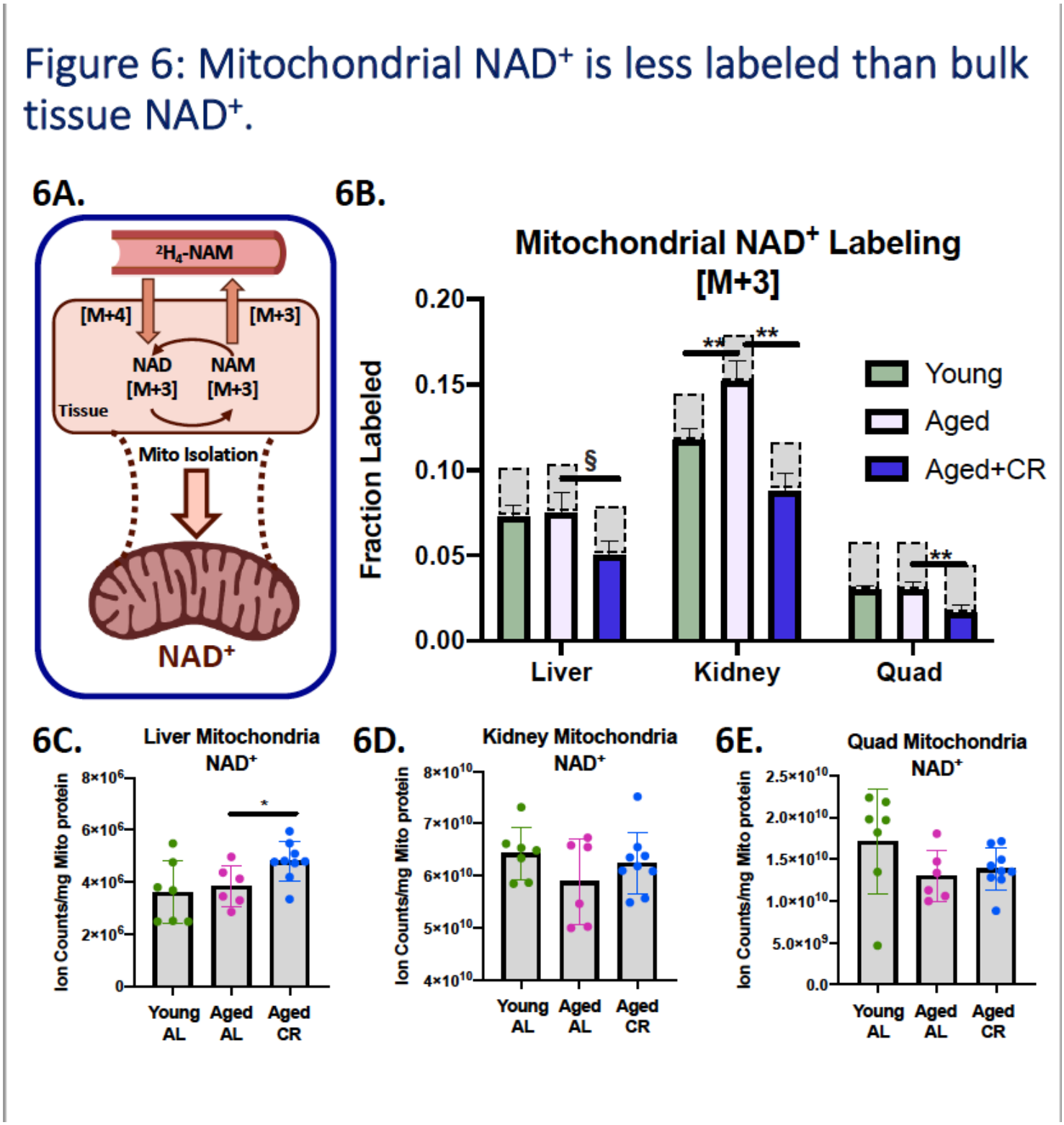

Figure 6

Mitochondria NAD+ is less labeled than bulk tissue NAD+. A, Schematic illustrating that intact tissues are labeled in vivo prior to mitochondrial isolation and NAD+ extraction. B., Mitochondria NAD+ turnover from circulating NAM—grey bars represent bulk tissue labeling. C-E, Mitochondria NAD+ pools in young, aged and aged +CR mice. Young, n=6; aged, n=6; aged+CR, n=7. For all panels, error bars indicate S.E.M. ***, $p < 0.001$; **, $p < 0.01$; *, $p < 0.05$; §, $p < 0.1$, calculated with Student's t-test.

Supplementary Files

This is a list of supplementary files associated with this preprint. Click to download.

- SuppFigures.pdf
- TableS1.docx